A robust statistical estimation (RoSE) algorithm jointly recovers the 3D location and intensity of single molecules accurately and precisely

Hesam Mazidi, Arye Nehorai, Matthew D. Lew

Hesam Mazidi, Arye Nehorai, Matthew D. Lew, "A robust statistical estimation (RoSE) algorithm jointly recovers the 3D location and intensity of single molecules accurately and precisely," Proc. SPIE 10500, Single Molecule Spectroscopy and Superresolution Imaging XI, 105000E (20 February 2018); doi: 10.1117/12.2289994

SPIE.

Event: SPIE BiOS, 2018, San Francisco, California, United States

A Robust Statistical Estimation (RoSE) algorithm jointly recovers the 3D location and intensity of single molecules accurately and precisely

Hesam Mazidi[a], Arye Nehorai[a], Matthew D. Lew*[a]
[a]Department of Electrical and Systems Engineering, Washington University in St. Louis,
1 Brookings Drive, St. Louis, MO, USA 63130

ABSTRACT

In single-molecule (SM) super-resolution microscopy, the complexity of a biological structure, high molecular density, and a low signal-to-background ratio (SBR) may lead to imaging artifacts without a robust localization algorithm. Moreover, engineered point spread functions (PSFs) for 3D imaging pose difficulties due to their intricate features. We develop a Robust Statistical Estimation algorithm, called RoSE, that enables joint estimation of the 3D location and photon counts of SMs accurately and precisely using various PSFs under conditions of high molecular density and low SBR.

Keywords: single-molecule localization microscopy, multi-dimensional reconstruction algorithm, joint sparsity, joint location and brightness estimation, 3D super-resolution fluorescence microscopy

1. INTRODUCTION

Fluorescence imaging and spectroscopy have been workhorse technologies in biological laboratories since their inception[1]. Labeling a specific biomolecule with a small organic dye or fluorescent protein enables single copies of these biomolecules to be detected as bright objects against a dark background within living cells[2,3]. The recent development of super-resolved fluorescence microscopy[4–6] magnifies the power and utility of these tools, enabling images of biological structures to be created with resolution beyond the diffraction limit of light (~250 nm for visible light). Single-molecule localization microscopy (SMLM) achieves this resolution by repeatedly localizing individual blinking fluorophores over time. The capabilities of SMLM are further augmented by its three-dimensional (3D) variants[7], where the point spread function (PSF), or optical response to a point emitter, is specifically designed to give 3D information from a 2D image captured by a camera. Indeed, SMLM is part of a modern trend in optics[8,9] that integrates computational algorithms with physical hardware in order to improve imaging performance.

The attainable resolution of SMLM is limited by the precision of localizing an individual molecule, termed localization precision[10–12], from Poissonian shot noise due to the finite number of photons detected from each molecule. Modern SM localization algorithms are capable of achieving the theoretical limit of localization precision[13–15]. Localization precision can be improved by utilizing brighter fluorophores[16–18], reducing photobleaching[19,20], and reducing background fluorescence within a sample. Further, the number and spatial distribution of molecular blinking events on the target structure can also limit the quality of reconstructed SMLM images[21,22]. SMLM imaging performance is also limited by the accuracy of localizing an individual molecule. Localization bias can result from model PSF mismatch[23] (e.g., arising from anisotropic molecular emission[14,24,25]), optical aberrations[26], and the image-processing algorithm[27] utilized to localize each molecule.

Recently, algorithms capable of localizing multiple overlapping molecules[28–31] have been utilized to decrease the time needed to acquire an SMLM dataset. However, they are optimized for specific optical PSFs and are not readily adaptable to analyze others. Here, we develop RoSE to accurately and precisely estimate the 3D location and brightness of SMs from microscopes utilizing a variety of 3D PSFs.

2. ROBUST STATISTICAL ESTIMATION

2.1 Forward model

We assume that within each imaging frame, no two molecules emit within a certain neighborhood. Therefore, the continuous position of a single molecule can be mapped to a distinct grid point in object space, where each point is associated with a brightness and a set of position gradients. Importantly, our signal model explicitly handles sub-pixel

*mdlew@wustl.edu; phone 1-314-935-6790; fax 1-314-935-7500; lewlab.wustl.edu

Single Molecule Spectroscopy and Superresolution Imaging XI, edited by Jörg Enderlein, Ingo Gregor, Zygmunt Karol Gryczynski, Rainer Erdmann, Felix Koberling, Proc. of SPIE Vol. 10500, 105000E
 · doi: 10.1117/12.2289994

shifts in the position of a molecule, whereas conventional brightness-only signal models cannot. This joint signal model together with a first-order approximation result in a linear forward imaging model with a convex set of constraints on the molecular parameters to be estimated, denoted as $\boldsymbol{\mathcal{O}} \in \mathbb{R}^{N\times 4}$, given by:

$$\boldsymbol{g} = \boldsymbol{A}\boldsymbol{\gamma} \tag{1}$$

$$\boldsymbol{A} = \left[\Phi, \boldsymbol{G}_x, \boldsymbol{G}_y, \boldsymbol{G}_z\right] \tag{2}$$

$$\boldsymbol{\gamma} = [\boldsymbol{s}^T, \boldsymbol{s}^T \odot \Delta\boldsymbol{x}^T, \boldsymbol{s}^T \odot \Delta\boldsymbol{y}^T, \boldsymbol{s}^T \odot \Delta\boldsymbol{z}^T] = \left[\boldsymbol{s}^T, \boldsymbol{p}_x^T, \boldsymbol{p}_y^T, \boldsymbol{p}_z^T\right] \tag{3}$$

$$\boldsymbol{\mathcal{O}} = \begin{bmatrix} s_1 & \Delta x_1 & \Delta y_1 & \Delta z_1 \\ s_2 & \Delta x_2 & \Delta y_2 & \Delta z_2 \\ \vdots & \vdots & \vdots & \vdots \\ s_N & \Delta x_N & \Delta y_N & \Delta z_N \end{bmatrix} \tag{4}$$

$$\boldsymbol{\mathcal{C}} = \left\{ s_i \geq 0, -s_i r_j \leq p_{j,i} < s_i r_j,\ i \in \{1, \dots, N\}, j \in \{x, y, z\} \right\} \tag{5}$$

where $\boldsymbol{g} \in \mathbb{R}^m$ represents the vectorized noiseless image relayed by the microscope; $\Phi \in \mathbb{R}^{m\times N}$ demotes the PSF matrix sampled at grid points; $\boldsymbol{G}_x \in \mathbb{R}^{m\times N}$, $\boldsymbol{G}_y \in \mathbb{R}^{m\times N}$, and $\boldsymbol{G}_z \in \mathbb{R}^{m\times N}$ represent corresponding gradient matrices along x, y, and z, respectively; N is the number of object grid points; and m is the number of image pixels. Further, $\boldsymbol{s} \in \mathbb{R}^N$ is the vectorized brightness and $\Delta\boldsymbol{x} \in \mathbb{R}^N$, $\Delta\boldsymbol{y} \in \mathbb{R}^N$, and $\Delta\boldsymbol{z} \in \mathbb{R}^N$ are the corresponding gradient vectors ($\odot$ represents component-wise multiplication of two vectors). Additionally, $\boldsymbol{\mathcal{C}}$ represents the convex set of constraints for a box centered at each grid point i with side lengths $2r_x$, $2r_y$, and $2r_z$ (Figure 1(a)).

2.2 Structured deconvolution

We first apply a structured deconvolution program to identify single molecules from their overlapping images. Our key insight is that the brightnesses $\boldsymbol{s}$ and position gradients $\left(\boldsymbol{G}_x, \boldsymbol{G}_y, \boldsymbol{G}_z\right)$ corresponding to single molecules are jointly sparse. That is, if the brightness of a molecule associated with a grid point is zero, then the corresponding position gradients should also be zero. The structured deconvolution is then cast as an optimization problem:

$$\min_{\boldsymbol{\gamma}\in\mathcal{C}} \mathcal{L}(\boldsymbol{\gamma}, \boldsymbol{A}; \boldsymbol{g}, \boldsymbol{b}) + \lambda\|\gamma\|_{1,2} \tag{6}$$

where $\mathcal{L}(\cdot)$ is the Poisson negative log likelihood function, $\|\cdot\|_{1,2}$ denotes the mixed $\ell_{1,2}$ norm to enforce joint sparsity, $\boldsymbol{b} \in \mathbb{R}^m$ is the vectorized background, and λ is a penalty parameter.

Figure 1(b) illustrates a 2D example of two closely-spaced molecules with significantly overlapping images. The molecular parameters $\boldsymbol{\mathcal{O}}$ recovered by Eqn. (6) cannot resolve the brightness and position of the two molecules. However, examining the joint structure of $\boldsymbol{\mathcal{O}}$ reveals that the brightness-weighted position gradients converge to the positions of each molecule. To make this mapping precise, we define a tensor $\boldsymbol{\mathcal{G}}$, called GradMap, in which each pixel, termed the source coefficient, takes on a value in $[-1,1]$ that signifies the local degree of convergence to that pixel (Figure 1(c)). Notably, GradMap leverages the convergent symmetry of the position gradients and does not require a symmetric PSF profile. Thus, the number of molecules and their initial parameters $\boldsymbol{\mathcal{O}}$ are estimated from the local maxima of GradMap (Figure 1(d)).

2.3 Adaptive maximum likelihood

After identifying the correct number of molecules via structured deconvolution, the errors in the initial estimates of their parameters need to be refined, as conventional sparse deconvolution programs exhibit systematic bias[30]. Interestingly, the distance between the true molecular position and the sparse recovery solution could be larger than a few grid points (Figure 1(e)). To restore accuracy, RoSE adaptively updates the grid point closest to the current estimate of the molecule's position by maximizing adaptively a constrained maximum likelihood. This strategy enhances the accuracy of both molecular position and brightness and attains the limits of precision indicated by the Cramér-Rao bound (CRB)[32].

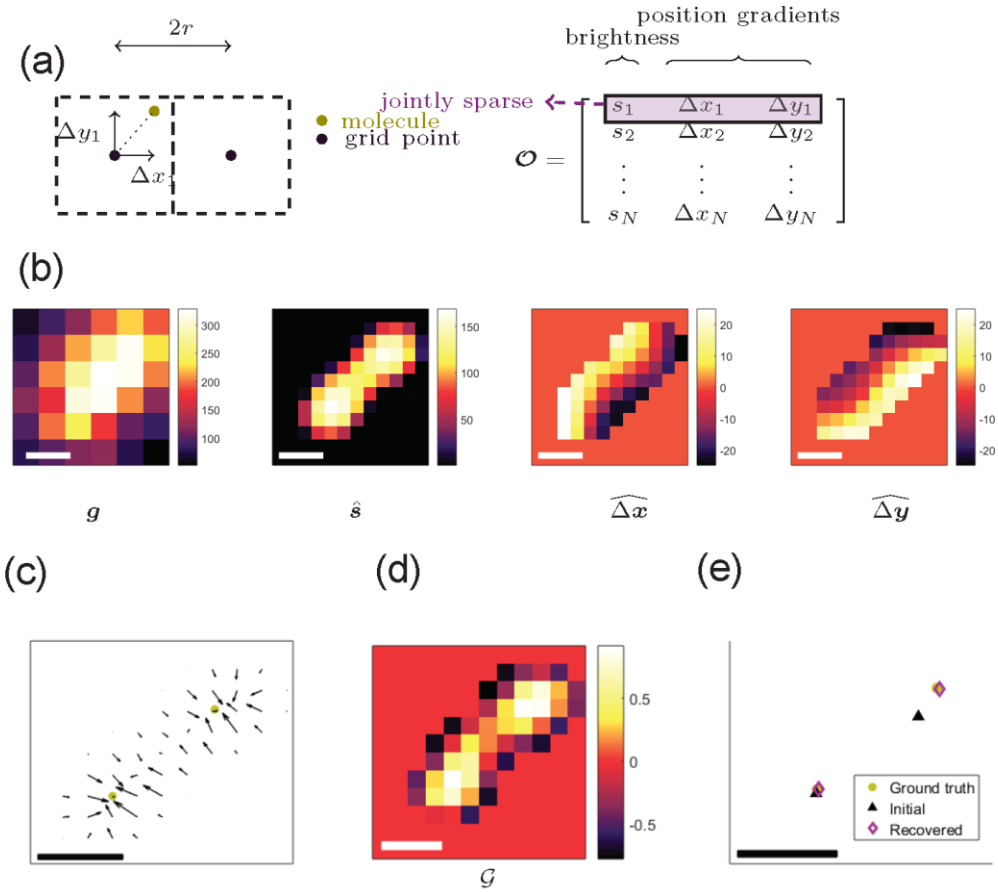

Figure 1. Joint recovery of molecular position and brightness by RoSE. (a) Joint signal model for molecular parameters in 2D, where s_i represents molecular brightness and $(\Delta x_i, \Delta y_i)$ represents the molecule's location relative to the nearest grid point. (b) Left: Simulated image of two overlapping molecules, located at (0,0) and (120,120) nm using the standard PSF. Right: Slices of recovered parameters $\boldsymbol{\mathcal{O}}$ by Eqns. (1)-(5). (c) Joint processing of brightness and position gradients of $\boldsymbol{\mathcal{O}}$ reveals two molecules unambiguously separated in 2D (green points). (d) Slice of estimated GradMap $\mathcal{G}$ at $z = 0$ for the recovered signal in (b). (e) Initial position estimates (black triangle) obtained via the GradMap in (c) and the recovered molecular positions (purple diamond) after applying adaptive constrained maximum likelihood compared to the ground-truth location of the two molecules (green points). Scale bars: 100 nm.

3. LOCALIZATION PRECISION AND ACCURACY

3.1 Localizing isolated molecules

To test the precision and accuracy of RoSE, we generated Poisson-distributed realizations of images $\boldsymbol{g}$ of single molecules located at various positions in 3D space using the tetrapod PSF[33]. The object grid ($r_x = r_y = 14.6$ nm, $r_z = 50$ nm) was sampled at twice the resolution of the camera (pixel size: 59.8 nm). For detected photon counts ranging from 722 to 10320, RoSE achieves CRB-limited localization precision (Figure 2) throughout a 3D depth range spanning $z \in [-1,1]$ μm.

We further tested the accuracy of RoSE specifically as a function of distance from the nearest grid point in object space. Since we use a first-order approximation of the PSF for our forward imaging model (Eqns. (1)-(3)), estimating the position and brightness of molecules near the boundary between grid points could incur significant bias. For 3D position measurements, we noticed no significant bias (the measured bias was much smaller than the CRB-limited precision) as a function of molecule position (Figure 3(a-c)). The photon-counting bias varied between undercounting and overcounting depending on the molecule's position from the grid (Figure 3(d)). However, this bias was well within the CRB-limited precision.

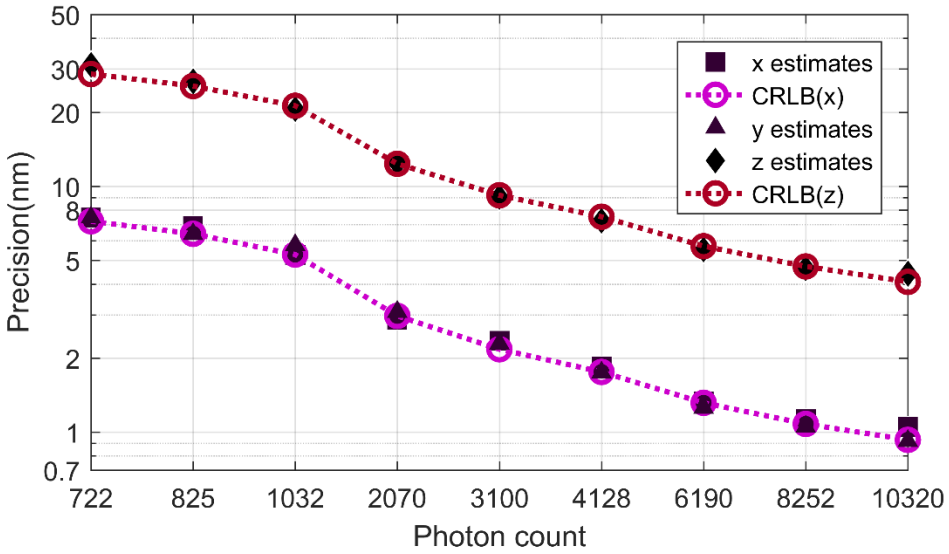

Figure 2. Localization precision of RoSE compared to CRB using the tetrapod PSF. The precision at each photon level was calculated from 200 measurements spread across a depth range spanning $z \in [-1,1]$ μm. A background level of 40 photons/pixel was used.

To ensure that ensemble measurements do not simply average competing biases to zero across the object domain, we examined the accuracy and covariance of position measurements at specific molecular positions $(x, y, z) = \{(0,0,0), (5,5,15), (10,10,30), (15,15,50)\}$ nm near the grid point $(x, y, z) = (0,0,0)$ nm and $(x, y, z) = \{(0,0,600), (5,5,615), (10,10,630), (15,15,650)\}$ nm near the grid point $(x, y, z) = (0,0,600)$ (Figure 4). At each molecular position, 200 noisy images were simulated at a signal level of 1032 photons and a background level of 40 photons/pixel. We compared RoSE's measurement statistics to $\sqrt{\text{CRB}}$ for precision and the ground-truth molecular location for accuracy.

Notably, the localization precision exhibited by RoSE closely matched the theoretical limit for all the tested positions, and the measured covariance matrices were essentially diagonal as expected. The accuracy of position estimates does become worse as the molecule's position moves away from the grid point, due to errors in the first-order approximation of our forward model, but the bias is well below the CRB-limited precision.

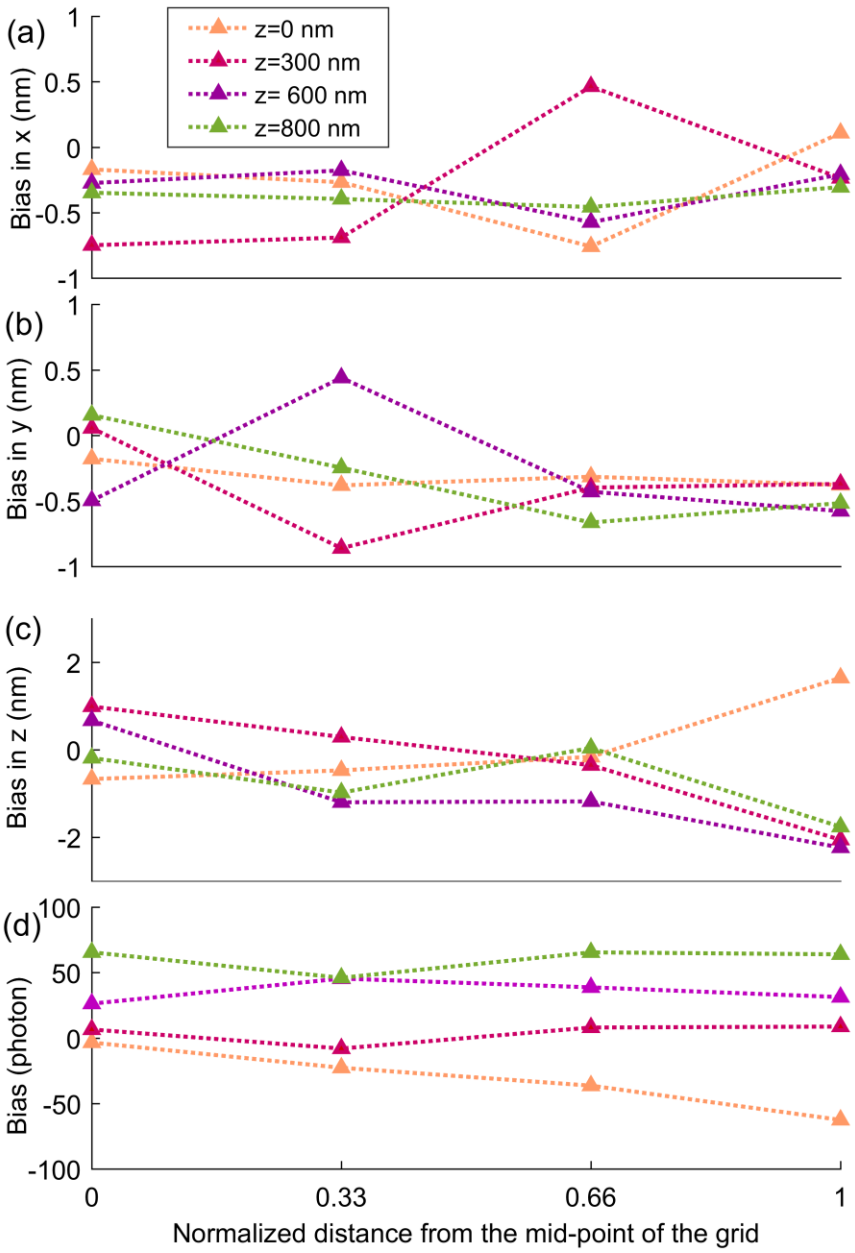

Figure 3. Bias of RoSE as a function of the molecule's lateral distance from the nearest grid point using the tetrapod PSF. Localization bias along (a) x, (b) y, and (c) z. (d) Photon-counting bias. Molecules were placed at $z = \{0\ (\text{orange}), 300\ (\text{red}), 600\ (\text{purple}), 800\ (\text{green})\}$ nm. The bias was calculated from 200 measurements at each position. A signal of 3100 photons and background level of 40 photons/pixel was used.

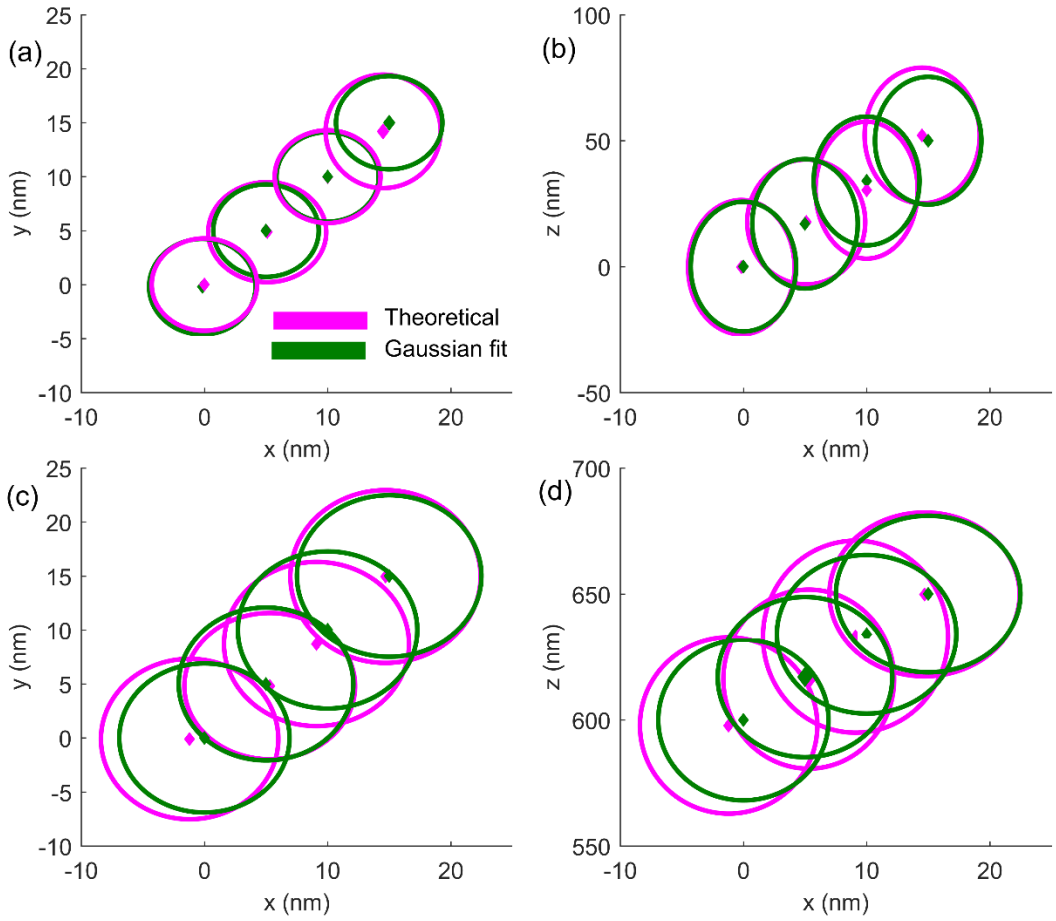

Figure 4. Localization bias and precision of RoSE as a function of molecular position using the tetrapod PSF. (a) Localization accuracy of RoSE (magenta diamond) compared to the ground truth molecular position (green diamond) within the xy plane ($z = 0$). The localization precision of RoSE (magenta ellipse) and $\sqrt{\text{CRB}}$ (green ellipse) are also shown. The object grid point is located at (0,0,0) nm. (b) Same as (a) but plotted in the xz plane. (c) Same as (a) but plotted for the xy plane at $z = 600$ nm. (d) Same as (c) but plotted in the xz plane. These data were calculated from 200 measurements at each position. A signal of 1032 photons and background level of 40 photons/pixel was used.

3.2 Localizing two closely-spaced molecules

We next tested the ability of RoSE to identify and localize pairs of molecules whose images overlap on the camera. In our simulations, the two molecules are separated laterally by 142 nm, and the axial position of the first molecule is held at $z = 0$, while the axial position of the second molecule is moved systematically. True positive, false positive, and false negative localizations were measured for 200 simulated images at each z position using the tetrapod PSF. An estimated location is assigned to the ground truth molecule if the following conditions hold:

$$\sqrt{(\hat{x} - x_{\text{true}})^2 + (\hat{y} - y_{\text{true}})^2} < 6\sqrt{\sigma_{x,\text{CRB}}^2 + \sigma_{y,\text{CRB}}^2} \tag{7}$$

$$\hat{z} - z_{\text{true}} < 6\sigma_{z,\text{CRB}} \tag{8}$$

Otherwise, the localized molecule is categorized as a false positive. We measured the precision and recall of RoSE (Figure 5) using the following definitions:

$$\text{Precision} = \frac{TP_1 + TP_2}{TP_1 + TP_2 + FP} \tag{9}$$

$$\text{Recall} = \frac{TP}{TP+FN} \tag{10}$$

where TP_i is the number of true positives for molecule i, FP is the number of false positives, and FN is the number of false negatives.

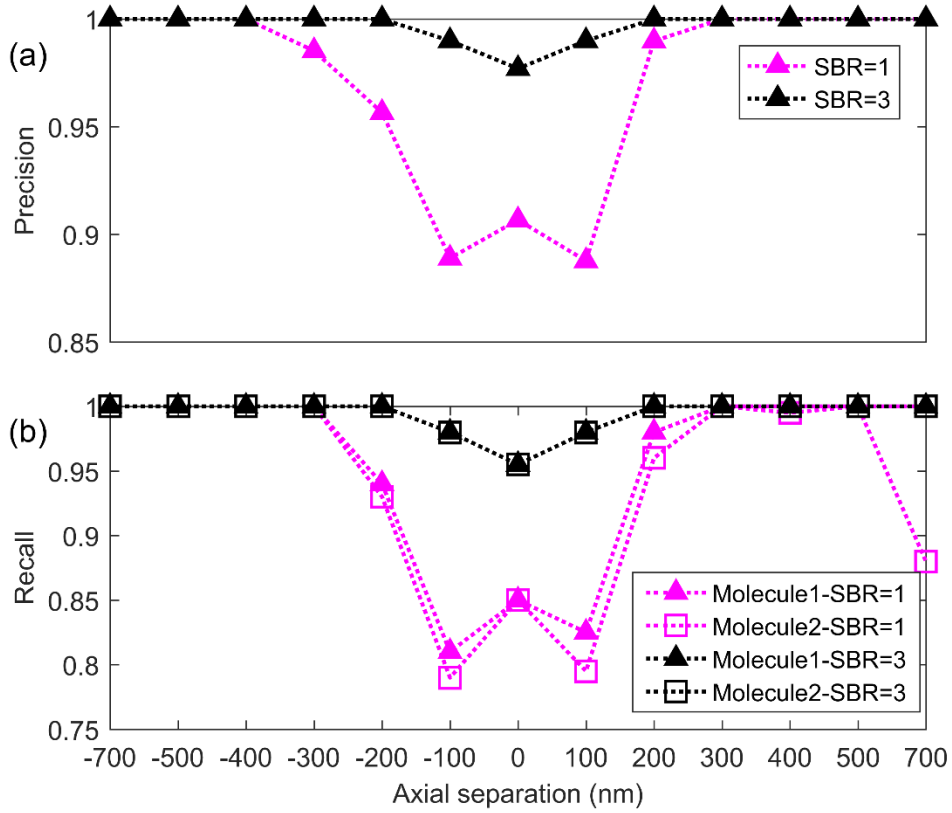

Figure 5. (a) Precision and (b) recall of localizing two closely-spaced molecules with a lateral separation of 142 nm using the tetrapod PSF. The axial position of molecule 1 was held fixed at $z = 0$, while the axial position of molecule 2 was varied systematically. SBR=1 (magenta curves) represents two molecules with 1032 photons detected and a background of 40 photons/pixel, while SBR=3 (black curves) represents 3100 photons detected and a background of 40 photons/pixel.

The measured precision is above 0.87 for all molecular separations for a signal-to-background (SBR) ratio of one, and the precision improves to above 0.98 for an SBR of three. In addition, the precision is unity for all z separations greater than 300 nm for both SBRs. The recall rate for each molecule is lower than the precision for both molecules, suggesting that RoSE tends to ignore overlapping molecules rather than mislocalize a molecule, thereby skewing toward false-negative errors rather than false-positive errors.

We next measured the lateral precision and bias of RoSE (Figure 6) in localizing two overlapping molecules. One molecule was placed at the origin, while the other molecule was placed at $(x_2, y_2) = (0,142)$ nm and a varying z position. RoSE achieves near CRB-limited localization precision for all tested z positions. Furthermore, biases of the estimates are within the CRB-limited localization precision, suggesting that the adaptive maximum likelihood is robust against systematic bias in the deconvolution step at various axial separations (Figure 6(b)).

Along the axial dimension, RoSE also achieves near CRB-limited localization precision for two closely-spaced molecules (Figure 7). We note the axial biases are larger compared to the lateral ones in Figure 6. This result can be attributed to the lower localization precision along z (Figure 7(a)) compared to the localization precision along y (Figure 6(a)) for the tetrapod PSF.

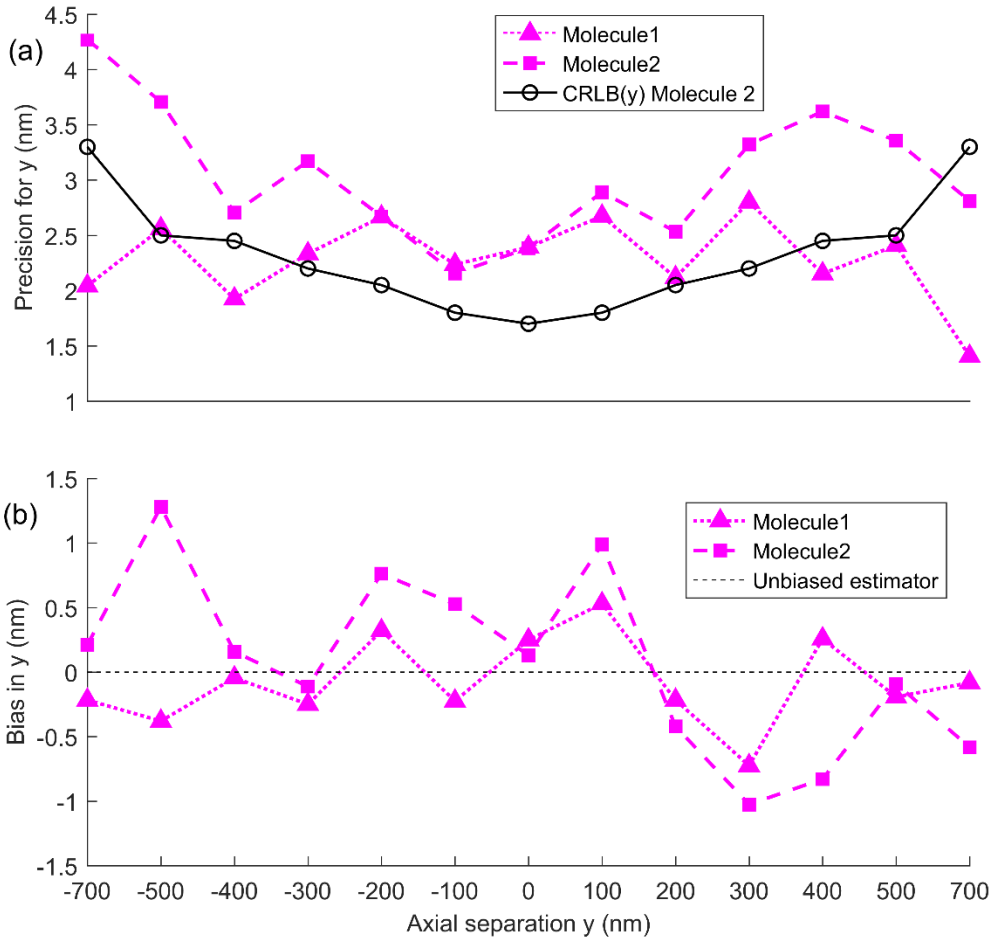

Figure 6. Lateral localization (a) precision and (b) bias of localizing two closely-spaced molecules located at $(x_1, y_1) = (0,0)$ nm and $(x_2, y_2) = (0,142)$ nm at an SBR of 3 corresponding to 3100 photons detected from each molecule with a background of 40 photons/pixel. Triangles (dotted curve) represent the precision and bias of localizing molecule 1, while squares (dashed curve) represent the precision and bias of localizing molecule 2. The ideal limits of localization precision and bias are plotted in black. A positive bias for molecule 1 indicates a bias toward the second molecule, while a negative bias for molecule 2 indicates a bias toward the first molecule.

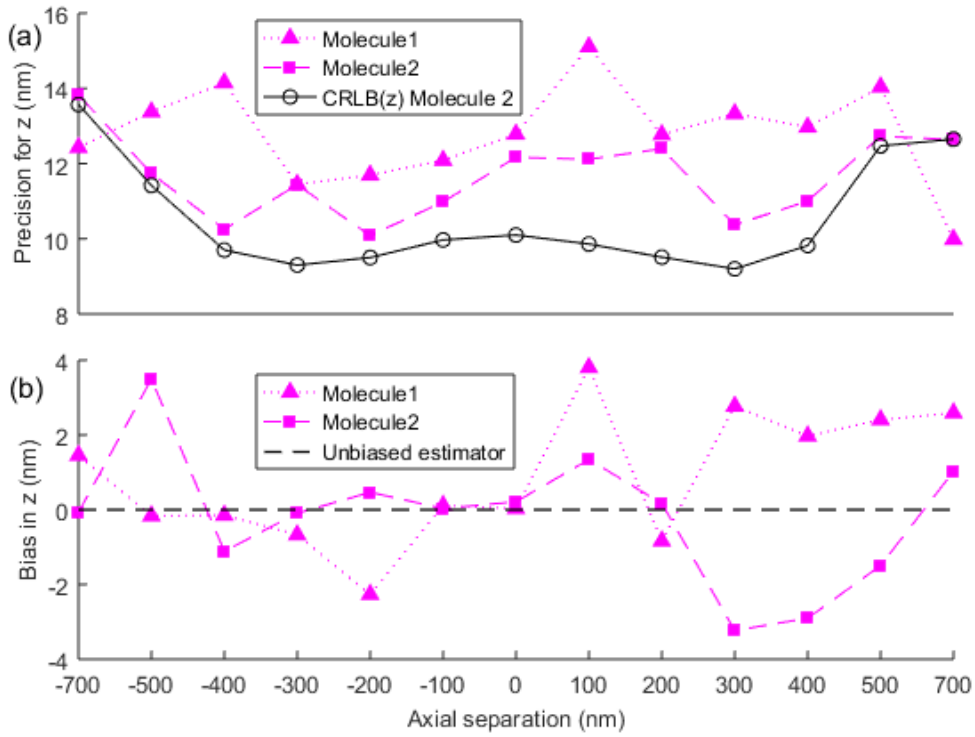

Figure 7. Axial localization (a) precision and (b) bias of localizing two closely-spaced molecules located at $(x_1, y_1) = (0,0)$ nm and $(x_2, y_2) = (0,142)$ nm at an SBR of 3 corresponding to 3100 photons detected from each molecule with a background of 40 photons/pixel. Triangles (dotted curve) represent the precision and bias of localizing molecule 1, while squares (dashed curve) represent the precision and bias of localizing molecule 2. The ideal limits of localization precision and bias are plotted in black.

4. CONCLUSION

We have demonstrated RoSE, a Robust Statistical Estimation algorithm, for localizing single molecules in high-density SMLM datasets using an arbitrary 3D PSF. A key feature of RoSE is its joint signal model, which allows blinking events to be localized with sub-pixel accuracy. RoSE achieves CRB-limited localization precision when localizing individual molecules and localizing pairs of overlapping molecules. In addition, the bias in RoSE measurements is insignificant compared to localization precision. In the future, RoSE will enable a single localization algorithm to be used across a variety of 3D microscopes and PSFs with minimal tuning or adaptation.

5. ACKNOWLEDGEMENTS

Research reported in this publication was supported by the National Science Foundation under grant number ECCS-1653777 and by the National Institute of General Medical Sciences of the National Institutes of Health under grant number R35GM124858.

REFERENCES

[1] Lakowicz, J. R., [Principles of Fluorescence Spectroscopy], Springer US, Boston, MA (2006).
[2] Moerner, W. E. and Fromm, D. P., "Methods of single-molecule fluorescence spectroscopy and microscopy," Rev. Sci. Instrum. **74**(8), 3597 (2003).
[3] Moerner, W. E., Shechtman, Y. and Wang, Q., "Single-molecule spectroscopy and imaging over the decades," Faraday Discuss. **184**, 9–36 (2015).
[4] Betzig, E., "Single Molecules, Cells, and Super-Resolution Optics (Nobel Lecture)," Angew. Chemie Int. Ed. **54**(28), 8034–8053 (2015).

[5] Hell, S. W., “Nanoscopy with Focused Light (Nobel Lecture),” Angew. Chemie Int. Ed. **54**(28), 8054–8066 (2015).
[6] Moerner, W. E., “Single-Molecule Spectroscopy, Imaging, and Photocontrol: Foundations for Super-Resolution Microscopy (Nobel Lecture),” Angew. Chemie Int. Ed. **54**(28), 8067–8093 (2015).
[7] von Diezmann, A., Shechtman, Y. and Moerner, W. E., “Three-Dimensional Localization of Single Molecules for Super-Resolution Imaging and Single-Particle Tracking,” Chem. Rev. **117**(11), 7244–7275 (2017).
[8] Zheng, G., Horstmeyer, R. and Yang, C., “Wide-field, high-resolution Fourier ptychographic microscopy,” Nat. Photonics **7**(9), 739–745 (2013).
[9] McLeod, E. and Ozcan, A., “Unconventional methods of imaging: computational microscopy and compact implementations,” Reports Prog. Phys. **79**(7), 76001 (2016).
[10] Thompson, R. E., Larson, D. R. and Webb, W. W., “Precise Nanometer Localization Analysis for Individual Fluorescent Probes,” Biophys. J. **82**(5), 2775–2783 (2002).
[11] Ram, S., Ward, E. S. and Ober, R. J., “Beyond Rayleigh’s criterion: a resolution measure with application to single-molecule microscopy.,” Proc. Natl. Acad. Sci. U. S. A. **103**(12), 4457–4462 (2006).
[12] Rieger, B. and Stallinga, S., “The Lateral and Axial Localization Uncertainty in Super-Resolution Light Microscopy,” ChemPhysChem **15**(4), 664–670 (2014).
[13] Abraham, A. V, Ram, S., Chao, J., Ward, E. S. and Ober, R. J., “Quantitative study of single molecule location estimation techniques,” Opt. Express **17**(26), 23352 (2009).
[14] Mortensen, K. I., Churchman, L. S., Spudich, J. a and Flyvbjerg, H., “Optimized localization analysis for single-molecule tracking and super-resolution microscopy,” Nat. Methods **7**(5), 377–381 (2010).
[15] Smith, C. S., Joseph, N., Rieger, B. and Lidke, K. a., “Fast, single-molecule localization that achieves theoretically minimum uncertainty,” Nat. Methods **7**(5), 373–375 (2010).
[16] Dempsey, G. T., Vaughan, J. C., Chen, K. H., Bates, M. and Zhuang, X., “Evaluation of fluorophores for optimal performance in localization-based super-resolution imaging,” Nat. Methods **8**(12), 1027–1036 (2011).
[17] Vaughan, J. C., Jia, S. and Zhuang, X., “Ultrabright photoactivatable fluorophores created by reductive caging,” Nat. Methods **9**(12), 1181–1184 (2012).
[18] Wang, S., Moffitt, J. R., Dempsey, G. T., Xie, X. S. and Zhuang, X., “Characterization and development of photoactivatable fluorescent proteins for single-molecule-based superresolution imaging,” Proc. Natl. Acad. Sci. **111**(23), 8452–8457 (2014).
[19] Rasnik, I., McKinney, S. a and Ha, T., “Nonblinking and long-lasting single-molecule fluorescence imaging.,” Nat. Methods **3**(11), 891–893 (2006).
[20] Zheng, Q., Juette, M. F., Jockusch, S., Wasserman, M. R., Zhou, Z., Altman, R. B. and Blanchard, S. C., “Ultra-stable organic fluorophores for single-molecule research,” Chem. Soc. Rev. **43**(4), 1044–1056 (2014).
[21] Shroff, H., Galbraith, C. G., Galbraith, J. A. and Betzig, E., “Live-cell photoactivated localization microscopy of nanoscale adhesion dynamics,” Nat. Methods **5**(5), 417–423 (2008).
[22] Nieuwenhuizen, R. P. J., Lidke, K. a., Bates, M., Puig, D. L., Grünwald, D., Stallinga, S. and Rieger, B., “Measuring image resolution in optical nanoscopy,” Nat. Methods **10**(6), 557–562 (2013).
[23] Deschout, H., Zanacchi, F. C., Mlodzianoski, M., Diaspro, A., Bewersdorf, J., Hess, S. T. and Braeckmans, K., “Precisely and accurately localizing single emitters in fluorescence microscopy,” Nat. Methods **11**(3), 253–266 (2014).
[24] Engelhardt, J., Keller, J., Hoyer, P., Reuss, M., Staudt, T. and Hell, S. W., “Molecular Orientation Affects Localization Accuracy in Superresolution Far-Field Fluorescence Microscopy,” Nano Lett. **11**(1), 209–213 (2011).
[25] Lew, M. D., Backlund, M. P. and Moerner, W. E., “Rotational mobility of single molecules affects localization accuracy in super-resolution fluorescence microscopy.,” Nano Lett. **13**(9), 3967–3972 (2013).
[26] von Diezmann, A., Lee, M. Y., Lew, M. D. and Moerner, W. E., “Correcting field-dependent aberrations with nanoscale accuracy in three-dimensional single-molecule localization microscopy.,” Optica **2**(11), 985–993 (2015).
[27] Sage, D., Kirshner, H., Pengo, T., Stuurman, N., Min, J., Manley, S. and Unser, M., “Quantitative evaluation of software packages for single-molecule localization microscopy,” Nat. Methods **12**(8), 717–724 (2015).
[28] Holden, S. J., Uphoff, S. and Kapanidis, A. N., “DAOSTORM: an algorithm for high- density super-resolution microscopy,” Nat. Methods **8**(4), 279–280 (2011).
[29] Zhu, L., Zhang, W., Elnatan, D. and Huang, B., “Faster STORM using compressed sensing,” Nat. Methods **9**(7), 721–723 (2012).

[30] Min, J., Vonesch, C., Kirshner, H., Carlini, L., Olivier, N., Holden, S., Manley, S., Ye, J. C. and Unser, M., "FALCON: fast and unbiased reconstruction of high-density super-resolution microscopy data," Sci. Rep. **4**(1), 4577 (2015).
[31] Gustafsson, N., Culley, S., Ashdown, G., Owen, D. M., Pereira, P. M. and Henriques, R., "Fast live-cell conventional fluorophore nanoscopy with ImageJ through super-resolution radial fluctuations," Nat. Commun. **7**, 12471 (2016).
[32] Kay, S. M., [Fundamentals of statistical signal processing], Prentice Hall, Englewood Cliffs, N.J. (1993).
[33] Shechtman, Y., Weiss, L. E., Backer, A. S., Sahl, S. J. and Moerner, W. E., "Precise Three-Dimensional Scan-Free Multiple-Particle Tracking over Large Axial Ranges with Tetrapod Point Spread Functions," Nano Lett. **15**(6), 4194–4199 (2015).